# Documentation of the Physical Core of the Bern3D Ocean Component

Stefan P. Ritz*

March 29, 2012

*ritz@climate.unibe.ch

# Contents

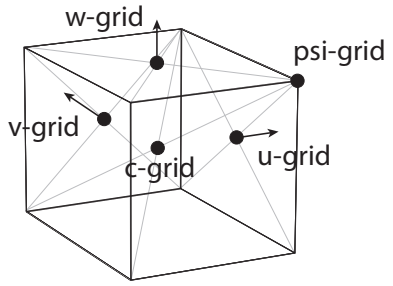


**Figure 1:** Illustration of the location of grid points on the c-, u-, v-, w-, and psi-grid with respect to a model cell.

# 1 Introduction

The basis of the physical core of the ocean component is described by Edwards et al. [1998]. The model has been updated through time. These major improvements are documented by Edwards and Shepherd [2002], Edwards and Marsh [2005], and Müller et al. [2006]. Additional details of the model description can be found in Müller [2007]. Although all necessary information required to understand the model can be found in the papers above and in references therein, a big effort has to be made in order to understand the Fortran model code, mainly because of the difficulty to find the equations in their discretized form within the model code.

In this documentation, all equations of the physical core of the ocean model are listed in their analytic form as well as in their discretized form. Also, it is noted in which subroutine the particular equations are found.

Note that the energy and moisture balance atmosphere component of the Bern3D model is described in Ritz et al. [2011a] with the detailed discretizations in Ritz [2011]. Adjustments to the energy and moisture balance atmosphere have been made since. They are listed in Appendix A of Ritz et al. [2011b].

## 1.1 Grid notation and indexing

When discretizing equations on to the model grid, it is very important to understand on which grid the quantities are discretized. Also, the indexing of each grid must be clear. Figure 1 depicts where the grid points of the various grids lie with respect to the model cell. Figures 2 and 3 depict the indexing of the $i$, $j$, and $k$ indices. The indexing is very important in the discretized equations. If a quantity can be located on more than one grid, a second index denotes the specific grid. $\theta^u_j$ for instance is the latitude at index $j$ on the u-grid.

## 1.2 Grid spacing

`gseto.F`

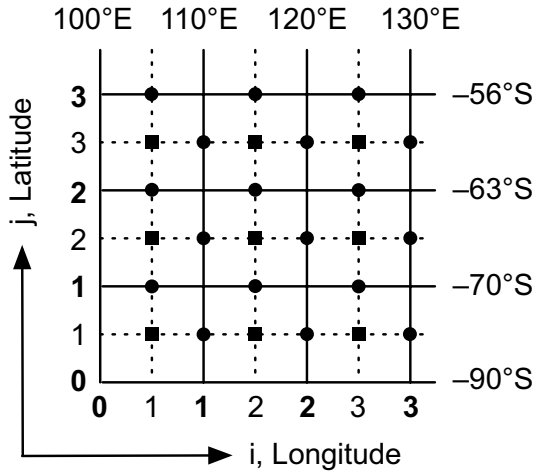


**Figure 2:** How the indices $i$ and $j$ are used on the grid of the Bern3D model. Solid lines and bold numbers indicate the borders of the grid cells, while dashed lines and regular numbers denote the centers of the grid cells. Tracers such as temperature and salinity are calculated at the center of each grid cell (squares, referred to as c-grid), the advective and diffusive fluxes are calculated at the edges (circles, referred to as u-grid and v-grid). The streamfunction is calculated at the box corners (psi-grid). Figure from Ritz [2011].

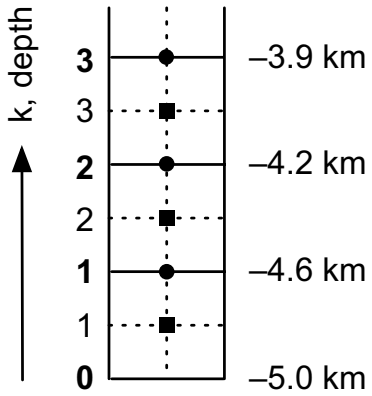


**Figure 3:** How the index $k$ is used on the grid of the Bern3D model. Solid lines and bold numbers indicate the borders of the grid cells, while dashed lines and regular numbers denote the centers of the grid cells.

In longitudinal direction, the world is partitioned into imax equally-spaced grid cells. $\Delta\phi = 2\pi/\text{imax}$ is the longitudinal angle between two cells. In latitudinal direction, the sine of the latitude is chosen to be equally spaced: $\Delta(\sin\theta) = 2/\text{jmax}$, where jmax are the number of cells in latitudinal direction. Due to this choice, the surface area of all cells is equal. In z-direction, the cell-height is chosen to increase exponentially with depth:

$$z_k^w = \eta \left[ \left(1 + \frac{1}{\eta}\right)^{\frac{\text{kmax}-k}{\text{kmax}}} - 1 \right] \cdot 5000\,\text{m}; \qquad k \in \{0, 1, \ldots, \text{kmax}\} \tag{1}$$

for the edges of the grid cells (on the w-grid) with $\eta = 0.1$, kmax the number of layers, and

$$z_k^c = \eta \left[ \left(1 + \frac{1}{\eta}\right)^{\frac{\text{kmax}-k+0.5}{\text{kmax}}} - 1 \right] \cdot 5000\,\text{m}; \qquad k \in \{1, 2, \ldots, \text{kmax}\} \tag{2}$$

for the "centers" of the grid cells (on the c-grid; note that these grid points are not actually located at the centers of the cells).

In the standard model version, imax=36, jmax=36, and kmax=32.

## 1.3 Gradient and divergence in spherical coordinates

The gradient and divergence operators in spherical coordinates are required in the model:

$$\nabla X = \left( \frac{1}{r\cos\theta}\frac{\partial}{\partial\phi}, \frac{\cos\theta}{r}\frac{\partial}{\partial(\sin\theta)}, \frac{\partial}{\partial z} \right) X\,, \tag{3}$$

$$\nabla \cdot \mathbf{X} = \left( \frac{1}{r}\frac{\partial}{\partial\phi}\frac{1}{\cos\theta}, \frac{1}{r}\frac{\partial}{\partial(\sin\theta)}\cos\theta, \frac{\partial}{\partial z} \right) \cdot \mathbf{X}\,. \tag{4}$$

Vectors and matrices are in indicated in bold letters throughout this documentation.

## 1.4 General remarks on discretizations in the Bern3D model

In order to understand the discretizations used in the model and in this documentation, the following general discretization rules must be understood.

The Bern3D model is designed such that the errors of the spatial discretizations are of second order except at one place where the error is larger (Section 2.1). Thus, the main spatial discretization scheme used is the centered differences scheme (also referred to as centered-in-space scheme; see e.g. Stocker [2011] for an introduction to the errors of discretization schemes). This is illustrated on the simple example of a diffusive flux in x-direction in the Cartesian coordinate system:

$$F^{\text{diff}} = -K\frac{\partial X}{\partial x}, \tag{5}$$

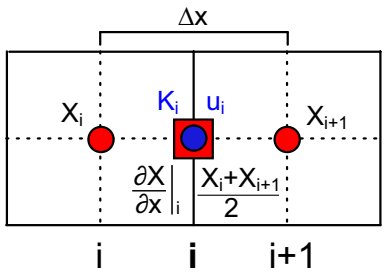


**Figure 4:** Example of a centered-in-space discretization in x-direction as in Eqs. (6) and (8). The tracer concentrations $X$ are located on the c-grid in the cell centers (red circles), whereas the velocity $u$ and the diffusion constant are located on the u-grid (blue circle). The derivative of $X$ with respect to $x$ is also located on the u-grid (as in Eq. 6) as well as the mean value of the two tracer concentrations (as in Eq. 8) (red square).

where $K$ is the diffusion constant, $X$ the tracer concentration, and $x$ the distance in x-direction. In the discretized form, this equation reads

$$F_i^{\text{diff}} = -K_i \frac{X_{i+1} - X_i}{\Delta x}, \tag{6}$$

where $\Delta x$ is the distance between the two tracer coordinates and $i$ the cell-index in x-direction. Because of the centered differences scheme, the derivative of $X$ lies on the u-grid between both concentrations $X_{i+1}$ and $X_i$ (Fig. 4). Because $K_i$ also lies on the u-grid, they can be multiplied.

In the example of an advective flux in x-direction

$$F^{\text{adv}} = uX, \tag{7}$$

the velocity $u$ which lies on the u-grid in discretized form must be multiplied with the tracer concentration which lies on the c-grid. When the centered-in-space scheme is used (as in most cases in the Bern3D model), the tracer concentrations of two adjacent cells must be averaged. The result is an averaged tracer concentration located on the u-grid that can be multiplied with the velocity:

$$F^{\text{adv}} = u_i \frac{X_i + X_{i+1}}{2} \tag{8}$$

(Fig. 4). Note that in the special case of advection, not the centered-in-space, but a weighted-upstream method is used, where depending on the flow direction and flow speed $u$, the tracer concentration upstream receives a greater weight than the tracer concentration downstream (see Section 3.1.1).

The temporal discretization scheme used in the Bern3D model is the Euler forward scheme (forward-in-time). Thus, the temporal discretization error is of first order.

**Table 1:** Constants of the discretized equations that do not appear in the model code due to the nondimensionalized form of the code.

| constant | variable name | description |
|---|---|---|
| $r$ | `rsc` | radius of the earth |
| $g$ | `gsc` | gravitational acceleration |
| $\rho_0$ | `rh0sc` | reference ocean density |
| $2\Omega$ | `fsc` | constant of the Coriolis parameter |

### 1.5 Nondimensionalized model code

Unfortunately, the physical core of the Bern3D model has been coded using nondimensionalized quantities. I.e., time $t$ is divided by a constant `tsc`, depth by a constant `dsc`, etc. In this documentation, all equations are written in their dimensionalized, physically correct form. When comparing the discretized equations of this documentation with the model code, certain constants will be missing in the model code because of its nondimensionalized form. These constants together with their variable name in the code are listed in Table 1.

## 2 Frictional geostrophic balance equations

The frictional geostrophic balance equations in spherical coordinates ($\phi \in [0; 2\pi]$, $\theta \in [-\pi; \pi]$, $z$: negative depth) are listed in Müller et al. [2006]:

$$-fv + \lambda u - \frac{\alpha}{\rho_0}\frac{\partial \tau_\phi}{\partial z} = -\frac{1}{\rho_0 r \cos\theta}\frac{\partial p}{\partial \phi}\,, \tag{9}$$

$$fu + \lambda v - \frac{\alpha}{\rho_0}\frac{\partial \tau_\theta}{\partial z} = -\frac{\cos\theta}{\rho_0 r}\frac{\partial p}{\partial (\sin\theta)}\,, \tag{10}$$

$$\frac{\partial p}{\partial z} = -g\rho(T, S)\,, \tag{11}$$

where $\mathbf{u} = (u, v, w)$ is the advective velocity, $\lambda$ is a drag coefficient, $\tau$ the wind stress, $\alpha$ a scaling factor for the wind stress, $f = 2\Omega \sin\theta$ the Coriolis parameter with $\Omega$ the Earth's angular velocity, $r$ the radius of the earth, $g$ the gravitational acceleration, $\rho_0$ a constant reference ocean density, and $\rho$ the local density, depending only on temperature $T$ and salinity $S$ [Winton and Sarachik, 1993]. The vertical velocity component $w$ follows from the continuity equation

$$\nabla \cdot \mathbf{u} = 0. \tag{12}$$

In order to improve numerical stability, the diagnosed velocities $\mathbf{u}$ are relaxed towards the velocities of the previous time step $\mathbf{u}'$ by solving

$$\frac{\partial \mathbf{u}}{\partial t} = \frac{1}{\beta}(\mathbf{u} - \mathbf{u}') \tag{13}$$

for $\mathbf{u}$, where $\beta$ is the relaxation time scale.

The velocity field $\mathbf{u}$ is solved by separating $\mathbf{u}$ into a barotropic (vertically averaged) and a baroclinic component: $\mathbf{u} = \bar{\mathbf{u}} + \tilde{\mathbf{u}}$. Both components are solved separately.

## 2.1 Solving for the baroclinic velocity

`velc.F`

To determine the baroclinic solution of the velocity, Equations (9) and (10) are solved for $u$ and $v$:

$$u = \frac{1}{f^2+\lambda^2}\left[f\left(\frac{\alpha}{\rho_0}\frac{\partial\tau_\theta}{\partial z} - \frac{\cos\theta}{\rho_0 r}\frac{\partial p}{\partial(\sin\theta)}\right) + \lambda\left(\frac{\alpha}{\rho_0}\frac{\partial\tau_\phi}{\partial z} - \frac{1}{\rho_0 r\cos\theta}\frac{\partial p}{\partial\phi}\right)\right] \tag{14}$$

and

$$v = \frac{1}{f^2+\lambda^2}\left[\lambda\left(\frac{\alpha}{\rho_0}\frac{\partial\tau_\theta}{\partial z} - \frac{\cos\theta}{\rho_0 r}\frac{\partial p}{\partial(\sin\theta)}\right) - f\left(\frac{\alpha}{\rho_0}\frac{\partial\tau_\phi}{\partial z} - \frac{1}{\rho_0 r\cos\theta}\frac{\partial p}{\partial\phi}\right)\right]. \tag{15}$$

Equations (14) and (15) are then differentiated with respect to $z$ whereby $\partial p/\partial z$ is replaced by the hydrostatic balance (Eq. 11):

$$\frac{\partial u}{\partial z} = \frac{1}{f^2+\lambda^2}\left[f\left(\frac{\alpha}{\rho_0}\frac{\partial^2\tau_\theta}{\partial z^2} + \frac{g\cos\theta}{\rho_0 r}\frac{\partial\rho}{\partial(\sin\theta)}\right) + \lambda\left(\frac{\alpha}{\rho_0}\frac{\partial^2\tau_\phi}{\partial z^2} + \frac{g}{\rho_0 r\cos\theta}\frac{\partial\rho}{\partial\phi}\right)\right] \tag{16}$$

and

$$\frac{\partial v}{\partial z} = \frac{1}{f^2+\lambda^2}\left[\lambda\left(\frac{\alpha}{\rho_0}\frac{\partial^2\tau_\theta}{\partial z^2} + \frac{g\cos\theta}{\rho_0 r}\frac{\partial\rho}{\partial(\sin\theta)}\right) - f\left(\frac{\alpha}{\rho_0}\frac{\partial^2\tau_\phi}{\partial z^2} + \frac{g}{\rho_0 r\cos\theta}\frac{\partial\rho}{\partial\phi}\right)\right]. \tag{17}$$

The baroclinic solution $\tilde{u}(z)$ (and analogously $\tilde{v}(z)$) can now be calculated by integrating the derivative from the seafloor (at depth $-H$) to depth $z$:

$$\tilde{u}(z) = \tilde{u}(-H) + \int_{-H}^{z}\frac{\partial u}{\partial z}dz \tag{18}$$

(Fig. 5). $\tilde{u}(-H)$ is unknown, but it can be calculated as follows:

$$u^*(z) = \tilde{u}(z) - \tilde{u}(-H), \tag{19}$$

and its integral over depth reads

$$\int_{-H}^{0} u^*(z) = -H\tilde{u}(-H) \tag{20}$$

(the depth-integral of the baroclinic component is zero by definition). Solving Eq. (20) for $\tilde{u}(-H)$ and using

$$u^*(z) = \int_{-H}^{z}\frac{\partial u}{\partial z}dz \tag{21}$$

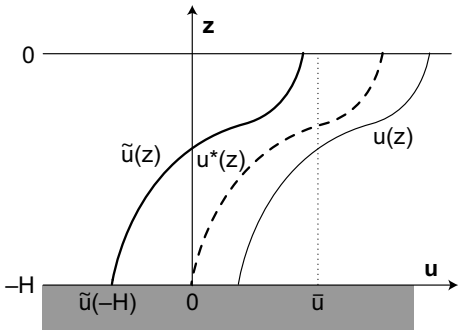


**Figure 5:** Illustration of the relationship between $\tilde{u}(z)$ and $u^*(z)$. $u^*(z) = \tilde{u}(z) - \tilde{u}(-H) = \int_{-H}^{z} \frac{\partial u}{\partial z} dz$.

leads to

$$\tilde{u}(-H) = -\frac{1}{H} \int_{-H}^{0} \int_{-H}^{z} \frac{\partial u}{\partial z} dz dz. \tag{22}$$

Hence,

$$\tilde{u}(z) = -\frac{1}{H} \int_{-H}^{0} \int_{-H}^{z} \frac{\partial u}{\partial z} dz dz + \int_{-H}^{z} \frac{\partial u}{\partial z} dz. \tag{23}$$

The boundary layer (or Ekman layer) stress is parametrized using a quadratic function with zero stress outside the boundary layer (hence $\boldsymbol{\tau}(D) = 0$ with $D$ the boundary layer thickness):

$$\boldsymbol{\tau}(z) = \frac{\boldsymbol{\tau}(0)}{D^2}(z + D)^2 \tag{24}$$

(Fig. 6)[1]. Accordingly, second derivative of $\boldsymbol{\tau}$ is

$$\frac{\partial^2 \boldsymbol{\tau}}{\partial z^2} = \frac{2\boldsymbol{\tau}(0)}{D^2}. \tag{25}$$

The boundary layer thickness $D$ is chosen to be one cell deep (about 39 m for kmax = 32). Note that according to Talley et al. [2011], $D$ is about 50 m.

### 2.1.1 Discretization

The components of Equation (16) are discretized as follows:

$$\frac{1}{\cos\theta} \frac{\partial \rho}{\partial \phi} = \frac{\rho_{i+1,j,k} - \rho_{i,j,k}}{\Delta\phi \cos\theta_j^u}, \tag{26}$$

$$\cos\theta \frac{\partial \rho}{\partial(\sin\theta)} = \cos\theta_j^u \frac{\rho_{i+1,j+1,k} - \rho_{i+1,j-1,k} + \rho_{i,j+1,k} - \rho_{i,j-1,k}}{4\Delta(\sin\theta)}, \tag{27}$$

[1]This suggestion of S. Ritz deviates from the parametrization of Edwards and Shepherd [2002], who suggest that the wind stress decreases linearly to zero over the uppermost grid cell. However, the second derivative of a linear decrease cannot be calculated properly.

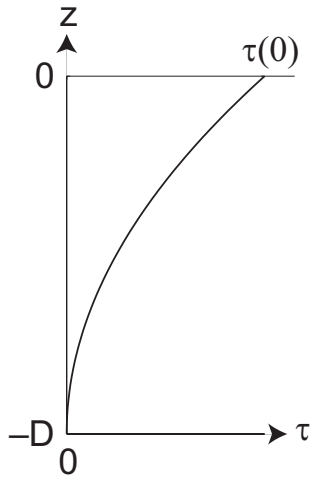


**Figure 6:** Parametrization of the stress $\boldsymbol{\tau}$ as a function of depth. Below the boundary layer of thickness $D$, the stress is zero. $\boldsymbol{\tau}(z) = \frac{\boldsymbol{\tau}(0)}{D^2}(z+D)^2$.

and

$$\frac{\partial^2 \tau}{\partial z^2} = \begin{cases} \frac{2\tau(0)}{[(\Delta z)^e_{\text{kmax}}]^2} & k = \text{kmax; as suggested by S. Ritz} \\ \frac{2\tau(0)}{(\Delta z)^e_{\text{kmax}}(\Delta z)^c_{\text{kmax}-1}} & k = \text{kmax; as in the current model code}^2 \\ 0 & \text{otherwise.} \end{cases} \tag{28}$$

$\rho_{i,j,k}$ is the density at cell $(i,j,k)$ (on the c-grid). $\theta^u_j$ is the latitude taken at index j on the u-grid. Since $\partial\tilde{u}/\partial z$ is on the u-grid, all components must be. The discretizations are done such that the derivatives of $\rho$ are located on the u-grid (see Fig. 7). Analogously for Equation (17) on the v-grid:

$$\frac{1}{\cos\theta}\frac{\partial \rho}{\partial \phi} = \frac{\rho_{i+1,j+1,k} - \rho_{i-1,j+1,k} + \rho_{i+1,j,k} - \rho_{i-1,j,k}}{\cos\theta^v_j \cdot 4\Delta\phi}\,, \tag{29}$$

$$\cos\theta\frac{\partial \rho}{\partial(\sin\theta)} = \cos\theta^v_j \frac{\rho_{i,j+1,k} - \rho_{i,j,k}}{\Delta(\sin\theta)}\,. \tag{30}$$

Note that there are special cases for Eqs. (27) and (29) if certain grid cells are not wet (not shown here). In these cases the discretization error is larger than second order. $(\Delta z)^e_{\text{kmax}}$ is the depth of the surface cell, and $(\Delta z)^c_{\text{kmax}-1}$ the distance between the centers of the two top model cells.

Equation (21) is discretized as

$$u^*_{i,j,k} = u^*_{i,j,k-1} + (\Delta z)^c_{k-1}\left.\frac{\partial u}{\partial z}\right|^e_{i,j,k-1} = u^*_{i,j,k-1} + (\Delta z)^c_{k-1}\frac{\left.\frac{\partial u}{\partial z}\right|^c_{i,j,k-1} + \left.\frac{\partial u}{\partial z}\right|^c_{i,j,k}}{2} \tag{31}$$

[2]The second derivative of the linear decrease of the wind stress is miraculously discretized to this value.

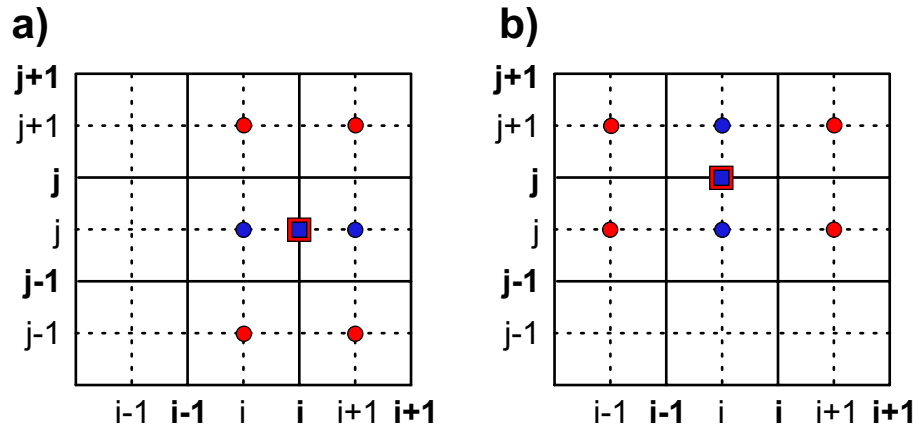


**Figure 7:** Visualization of discretizations. The circles denote the individual densities, the squares the resulting derivative. a) Eqs. (26) (blue) and (27) (red). b) Eqs. (29) (red) and (30) (blue).

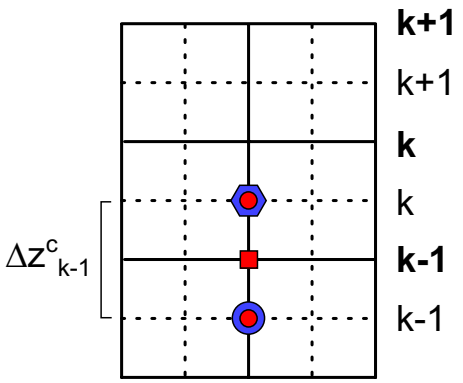


**Figure 8:** Visualization of the discretization of Eq. (31). The blue circle denotes the known velocity, red circles denote the depth-derivatives of u. The red square is the averaged depth-derivative. The blue polygon is the velocity that follows from the velocity below and from the derivatives.

and analogously for $\tilde{v}_{i,j,k}$ (see Fig. 8). $c$ denotes the quantity evaluated at the center of the cell with respect to depth, $e$ denotes the quantity evaluated at the edge of the cell. $(\Delta z)^c_{k-1}$ is the distance between the center of cell $k$ and the center of cell $k-1$. Because $\partial u/\partial z$ and $\partial v/\partial z$ are evaluated at the center of the cells (Eqs. 16 and 17), an averaging is done to calculate the derivative at the edge of the cell. Note that this non-weighted averaging is valid in second-order approximation (see Appendix A). Eq. (22) is discretized as

$$\frac{1}{H}\int_{-H}^{0} u^*(z)dz = \frac{1}{H^u_{i,j}} \sum_{n=\mathrm{kmin}}^{\mathrm{kmax}} u^*_{i,j,n} \cdot (\Delta z)^e_n, \tag{32}$$

where $H^u_{i,j}$ is the ocean depth on the u-grid, i.e. the depth of the deepest point where both adjacent cells are still wet. kmin is the index of this cell.

## 2.2 Solving for the barotropic velocity

`ubarsolv.F; wind.F; jbar.F; invert.F; island.F; matinv.F`

The barotropic (vertically integrated) component of the velocity field is calculated by first calculating the barotropic streamfunction $\Psi$ by solving

$$\frac{1}{r^2}J\left(\Psi,\frac{f}{H}\right)+\frac{1}{r^2}J\left(E,\frac{1}{H}\right)+\nabla\cdot\left(\frac{\lambda}{H}\nabla\Psi\right)-\mathbf{k}\cdot\nabla\times\left(\frac{\alpha\boldsymbol{\tau}(0)}{H}\right)=0\,, \tag{33}$$

for $\Psi$, where

$$E=g\int_{-H}^{0}z\rho dz\,, \tag{34}$$

$J(A,B)=\partial A/\partial\phi\cdot\partial B/\partial(\sin\theta)-\partial A/\partial(\sin\theta)\cdot\partial B/\partial\phi$ is the Jacobian, and $\mathbf{k}=(0,0,1)$. Eq. (33) can be determined by cross-differentiating the depth-averaged version of Eqs. (9) and (10) to eliminate the pressure terms (thereby using integration by parts and Eq. 11), and by using the relationship between the barotropic velocity $\bar{\mathbf{u}}$ and $\Psi$:

$$H\bar{\mathbf{u}}=\int_{-H}^{0}\mathbf{u}dz=\frac{1}{\rho_0}\mathbf{k}\times\nabla\Psi. \tag{35}$$

Note that

$$\int_{-H}^{0}\frac{\partial\boldsymbol{\tau}}{\partial z}dz=\boldsymbol{\tau}(0), \tag{36}$$

because the stress is zero outside the boundary layer where the stress acts. Thus, $\boldsymbol{\tau}(-H)=0$. The first term of Eq. (33) is the planetary vorticity advection (referred to as Coriolis term, calculated in `invert.F`, see Section 2.2.3), the second term represents the topographic forcing referred to as the joint effect of baroclinicity and relief, JEBAR, calculated in `jbar.F`, Section 2.2.1), the third term is the drag term (`invert.F`, Section 2.2.4), and the fourth term represents the wind stress forcing (calculated in `wind.F`, Section 2.2.2).

### 2.2.1 JEBAR

`jbar.F`

The second forcing term of Eq. (33) is greater than 0 when isopycnals above the topographic slope are not parallel to the isobaths. The term can be re-written to

$$\frac{1}{r^2}J\left(E,\frac{1}{H}\right)=\frac{1}{r^2}\left(\frac{\partial E}{\partial\phi}\frac{\partial\frac{1}{H}}{\partial(\sin\theta)}-\frac{\partial E}{\partial(\sin\theta)}\frac{\partial\frac{1}{H}}{\partial\phi}\right) \tag{37}$$

which in turn is discretized as follows:

$$\begin{aligned}\frac{\partial E}{\partial\phi}\frac{\partial\frac{1}{H}}{\partial(\sin\theta)}&=\frac{\partial E}{\partial\phi}\frac{1}{\Delta(\sin\theta)}\left(\frac{1}{H^u_{i,j+1}}-\frac{1}{H^u_{i,j}}\right)\\&=\frac{1}{\Delta\phi\Delta(\sin\theta)}\left[(E_{i+1,j+1}-E_{i,j+1})\frac{1}{H^u_{i,j+1}}-(E_{i+1,j}-E_{i,j})\frac{1}{H^u_{i,j}}\right],\end{aligned} \tag{38}$$

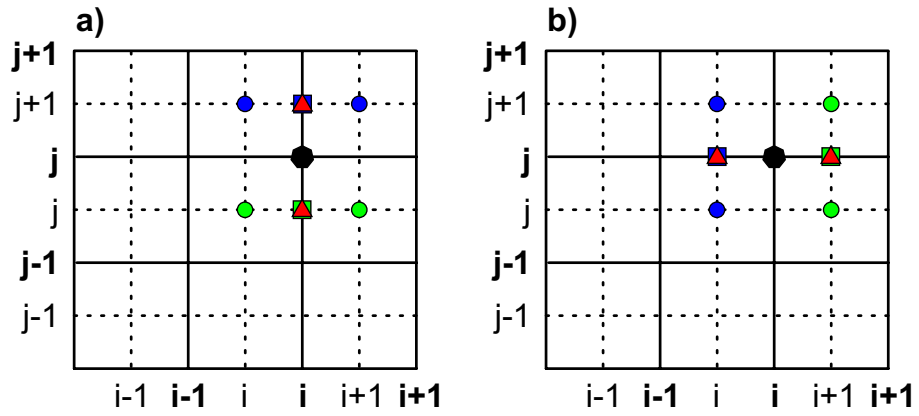


**Figure 9:** Visualization of the discretization of Eqs. (38) (a) and (39) (b). Circles denote the $E$-values, squares denote derivatives of $E$, triangles denote locations where the depth $H$ is taken, and the polygon denotes the location of the resulting term.

$$\begin{aligned}\frac{\partial E}{\partial(\sin\theta)}\frac{\partial\frac{1}{H}}{\partial\phi} &= \frac{\partial E}{\partial(\sin\theta)}\frac{1}{\Delta\phi}\left(\frac{1}{H^v_{i,j}}-\frac{1}{H^v_{i+1,j}}\right)\\ &= \frac{1}{\Delta\phi\Delta(\sin\theta)}\left[(E_{i,j+1}-E_{i,j})\frac{1}{H^v_{i,j}}-(E_{i+1,j+1}-E_{i+1,j})\frac{1}{H^v_{i+1,j}}\right]\end{aligned} \tag{39}$$

(see also Fig. 9). Using the hydrostatic balance (11), $E$ (Eq. 34) can be integrated by parts to

$$E = g\int_{-H}^{0} z\rho dz = -zp|_{-H}^{0} - g\int_{-H}^{0}\int_{-H}^{0}\rho(dz)^2 = -Hp(-H)+\int_{-H}^{0} pdz. \tag{40}$$

In the model code, $p$ is replaced by $p'$ with $p'(z)=p(z)-p(-H)$. Hence, $p'(-H)=0$ and

$$E = \int_{-H}^{0} p'dz. \tag{41}$$

In discretized form, $p'(z)$ is calculated by integrating the density from the sea floor to depth $z$ (analogously to Eq. 31):

$$p'_{i,j,k} = p'_{i,j,k-1} - g\frac{\rho_{i,j,k}+\rho_{i,j,k-1}}{2}(\Delta z)^c_{k-1} \tag{42}$$

with $p'_{i,j,\mathrm{kmin}} = 0$ and kmin being the k-index of the bottom-most wet cell. Again, the non-weighted averaging is valid in second-order approximation (Appendix A).

$$E_{i,j} = \sum_{n=\mathrm{kmin}^*}^{\mathrm{kmax}} p'_{i,j,n}\cdot(\Delta z)^e_n \tag{43}$$

with kmax the k-index of the top-most cell (at the sea surface) and kmin* the bottom-most wet grid point on the u- and v-grid, respectively, i.e. where the derivatives of $E$ are calculated (Fig. 10).

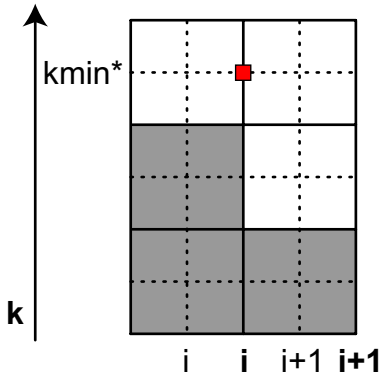


**Figure 10:** Index kmin* of Eq. (43). Because the derivatives of $E$ are located on the u- and v-grids, respectively, the integral of the pressure over depth (Eqs. (41) and (43) is calculated from the maximum depth $-H$ (k-index kmin*) where both adjacent cells are wet (red square).

### 2.2.2 The wind stress term

`wind.F`

The fourth term in Eq. (33)

$$\mathbf{k}\cdot\nabla\times\left(\frac{\alpha\boldsymbol{\tau}(0)}{H}\right)=\alpha\left(\frac{1}{r\cos\theta}\frac{\partial}{\partial\phi}\frac{\tau_\theta(0)}{H}-\frac{1}{r}\frac{\partial}{\partial(\sin\theta)}\cos\theta\frac{\tau_\phi(0)}{H}\right) \tag{44}$$

is discretized as follows:

$$\begin{aligned}\mathbf{k}\cdot\nabla\times\left(\frac{\alpha\boldsymbol{\tau}(0)}{H}\right)=&\frac{\alpha}{r}\left[\frac{1}{\cos\theta^v_j\Delta\phi}\left(\frac{\tau^v_{i+1,j}}{H^v_{i+1,j}}-\frac{\tau^v_{i,j}}{H^v_{i,j}}\right)\right.\\&\left.-\frac{1}{\Delta(\sin\theta)}\left(\frac{\tau^u_{i,j+1}\cos\theta^u_{j+1}}{H^u_{i,j+1}}-\frac{\tau^u_{i,j}\cos\theta^u_j}{H^u_{i,j}}\right)\right].\end{aligned} \tag{45}$$

### 2.2.3 The Coriolis term

`invert.F`

With $f=2\Omega\sin\theta$, the components of the first term in Eq. (33),

$$\frac{1}{r^2}J\left(\Psi,\frac{2\Omega\sin\theta}{H}\right)=\frac{2\Omega}{r^2}\left(\frac{\partial\Psi}{\partial\phi}\frac{\partial}{\partial(\sin\theta)}\frac{\sin\theta}{H}-\sin\theta\frac{\partial\Psi}{\partial(\sin\theta)}\frac{\partial}{\partial\phi}\frac{1}{H}\right), \tag{46}$$

are discretized as follows:

$$\frac{\partial\Psi}{\partial(\sin\theta)}=\frac{\Psi_{i,j+1}-\Psi_{i,j-1}}{2\Delta(\sin\theta)}, \tag{47}$$

$$\frac{\partial}{\partial\phi}\frac{1}{H}=\frac{1}{\Delta\phi}\left(\frac{1}{H^v_{i+1,j}}-\frac{1}{H^v_{i,j}}\right), \tag{48}$$

$$\frac{\partial\Psi}{\partial\phi}=\frac{\Psi_{i+1,j}-\Psi_{i-1,j}}{2\Delta\phi}, \tag{49}$$

and

$$\frac{\partial}{\partial(\sin\theta)}\frac{\sin\theta}{H} = \frac{1}{\Delta(\sin\theta)}\left(\frac{\sin\theta^u_{j+1}}{H^u_{i,j+1}} - \frac{\sin\theta^u_j}{H^u_{i,j}}\right). \tag{50}$$

### 2.2.4 The drag term

`invert.F`

The components of the third term in Eq. (33),

$$\nabla\cdot\left(\frac{\lambda}{H}\nabla\Psi\right) = \frac{1}{r^2\cos^2\theta}\frac{\partial}{\partial\phi}\left(\frac{\lambda}{H}\frac{\partial\Psi}{\partial\phi}\right) + \frac{1}{r^2}\frac{\partial}{\partial(\sin\theta)}\left(\cos^2\theta\frac{\lambda}{H}\frac{\partial\Psi}{\partial(\sin\theta)}\right), \tag{51}$$

are discretized as follows:

$$\frac{1}{r^2\cos^2\theta}\frac{\partial}{\partial\phi}\left(\frac{\lambda}{H}\frac{\partial\Psi}{\partial\phi}\right) = \frac{1}{r^2\cos^2\theta^v_j(\Delta\phi)^2}\left[\frac{\lambda^v_{i+1,j}}{H^v_{i+1,j}}(\Psi_{i+1,j}-\Psi_{i,j}) - \frac{\lambda^v_{i,j}}{H^v_{i,j}}(\Psi_{i,j}-\Psi_{i-1,j})\right], \tag{52}$$

and

$$\begin{aligned}\frac{1}{r^2}\frac{\partial}{\partial(\sin\theta)}\left(\cos^2\theta\frac{\lambda}{H}\frac{\partial\Psi}{\partial(\sin\theta)}\right) = \frac{1}{r^2\Delta(\sin\theta)^2}\Bigg[&\cos^2\theta^c_{j+1}\frac{\lambda^u_{i,j+1}}{H^u_{i,j+1}}(\Psi_{i,j+1}-\Psi_{i,j})\\ &-\cos^2\theta^c_j\frac{\lambda^u_{i,j}}{H^u_{i,j}}(\Psi_{i,j}-\Psi_{i,j-1})\Bigg].\end{aligned} \tag{53}$$

### 2.2.5 Solving for the barotropic streamfunction

`invert.F`

Equation (33) is solved for $\Psi$ implicitly: The equation can be written as

$$\mathbf{M}\boldsymbol{\Psi} = \mathbf{b}, \tag{54}$$

where $\boldsymbol{\Psi} = (\Psi_{0,0}, \Psi_{1,0}, \ldots, \Psi_{\mathrm{imax},0}, \Psi_{0,1}, \ldots, \Psi_{\mathrm{imax,jmax}})^T$. Matrix $\mathbf{M}$ contains the coefficients of the Coriolis and the drag terms (that are dependent on $\Psi$), whereas $\mathbf{b}$ contains the JEBAR and wind stress terms which do not depend on $\Psi$. Hence,

$$\boldsymbol{\Psi} = \mathbf{M}^{-1}\mathbf{b}. \tag{55}$$

Because the elements of $\mathbf{M}$ change seasonally but not inter-annually, the matrix needs to be inverted only during the first model year. Because $\mathbf{M}$ is a banded matrix, an inversion method for banded matrices is used to increase computational efficiency.

The matrix is set up and inverted in `invert.F`. Equation (55) is calculated in `ubarsolv.F`.

### 2.2.6 Solving for the barotropic velocity

`ubarsolv.F`

$\bar{\mathbf{u}}$ follows from $\Psi$ according to Eq. (35):

$$\bar{\mathbf{u}} = \frac{1}{\rho_0 H}\left(-\frac{\cos\theta}{r}\frac{\partial\Psi}{\partial(\sin\theta)}, \frac{1}{r\cos\theta}\frac{\partial\Psi}{\partial\phi}, 0\right) \tag{56}$$

and in the discretized form:

$$\bar{u}_{i,j} = -\frac{\cos\theta^u_j(\Psi_{i,j} - \Psi_{i,j-1})}{\rho_0 H^u_{i,j} r\Delta(\sin\theta)} \tag{57}$$

and

$$\bar{v}_{i,j} = \frac{\Psi_{i,j} - \Psi_{i-1,j}}{\rho_0 H^v_{i,j} r\cos\theta^v_j \Delta\phi}. \tag{58}$$

### 2.2.7 Treatment of islands and straits

`ubarsolv.F, island.F, matinv.F, mains.F`

The calculation of $\Psi$ and $\bar{\mathbf{u}}$ discussed so far is valid when the world consists of no islands except the mainland. However, additional terms arise when islands are introduced. In this case, $\Psi$ and $\bar{\mathbf{u}}$ are decomposed into several components:

$$\Psi = \Psi_I + \sum_{i=1}^{n}\Psi^i_B, \tag{59}$$

and

$$\bar{\mathbf{u}} = \bar{\mathbf{u}}_\mathbf{I} + \sum_{i=1}^{n}\bar{\mathbf{u}}^\mathbf{i}_\mathbf{B}, \tag{60}$$

where $\Psi_I$ and $\bar{\mathbf{u}}_\mathbf{I}$ represent the streamfunction and barotropic velocity due to the wind stress and JEBAR ocean interior forcing with $\Psi = 0$ at the ocean margins (as discussed in Sections 2.2.5 and 2.2.6). $\Psi^i_B$ and $\bar{\mathbf{u}}^\mathbf{i}_\mathbf{B}$ represent the boundary conditions of island $i$. There are $n$ islands apart from the mainland. $\Psi$ is not necessarily 0 at the island boundaries because there can be flow around the island.

$\Psi^i_B$ is calculated as $\Psi_I$ (Section 2.2.5) but by setting wind stress and JEBAR forcing to zero and by applying unit forcing at the ocean margin around island $i$ (i.e. $b_m = 1$ in Eq. (54) for the margin of island $i$ and 0 otherwise). The resulting $\Psi^{i*}_B$ and $\bar{\mathbf{u}}^{i*}_\mathbf{B}$ are then multiplied by a constant $c_i$ such that $\Psi^i_B = c_i\Psi^{i*}_B$ and $\bar{\mathbf{u}}^i_\mathbf{B} = c_i\bar{\mathbf{u}}^{i*}_\mathbf{B}$ in order to fulfill the rule that the depth-averaged momentum equations around the island must integrate to zero:

$$\begin{aligned}\sum_{C_u}\int_{C_u}\left(\lambda\bar{u} - f\bar{v} - \frac{\alpha\tau_\phi(0)}{\rho_0 H} + \frac{1}{Hr\rho_0}\int_{-H}^{0}\frac{1}{\cos\theta}\frac{\partial p}{\partial\phi}dz\right)\cos\theta d\phi \\ + \sum_{C_v}\int_{C_v}\left(\lambda\bar{v} + f\bar{u} - \frac{\alpha\tau_\theta(0)}{\rho_0 H} + \frac{1}{Hr\rho_0}\int_{-H}^{0}\cos\theta\frac{\partial p}{\partial(\sin\theta)}\right)\frac{1}{\cos\theta}d(\sin\theta) = 0,\end{aligned} \tag{61}$$

where the $C_u$ and $C_v$ are sections of the closed path $C$ in zonal and meridional direction, respectively. The calculation of constant $c$ is explained in the following. Note that $\Psi$ can be chosen to be zero at the mainland margin without loss of generality.

The calculation of the constants is explained based on an example of a world that consists of the mainland and three islands (e.g. mainland Eurasia and islands Antarctica, Australia, and America).

The path integral (61) around island $j$ (Australia for instance) can be split up into the path integral $\gamma_I^j$ that is calculated from the wind stress and ocean interior forcing using the velocity field $\bar{\mathbf{u}}_\mathbf{I}$, and the path integrals $\gamma_B^{ij}$ of the velocity fields $c_i \bar{\mathbf{u}}_\mathbf{B}^{i*}$ that are invoked by the boundary conditions of the three islands ($n = 3$ in this example):

$$\gamma_I^j + \sum_{i=1}^{n} \gamma_B^{ij} = 0 \tag{62}$$

with $j$ the island index (Australia for now) and

$$\gamma_B^{ij} = \sum_{C_u^j} \int_{C_u^j} (\lambda c_i \bar{u}_B^{i*} - f c_i \bar{v}_B^{i*}) \cos\theta d\phi + \sum_{C_v^j} \int_{C_v^j} (\lambda c_i \bar{v}_B^{i*} + f c_i \bar{u}_B^{i*}) \frac{1}{\cos\theta} d(\sin\theta) \tag{63}$$

with $C^j$ the closed path around island $j$. $c_i$ can be factored out, so Eq. (62) can be re-written as

$$\gamma_I^j + c_1 \gamma_B^{1j*} + c_2 \gamma_B^{2j*} + c_3 \gamma_B^{3j*} = 0 \tag{64}$$

with $\gamma_B^{ij*} = \gamma_B^{ij}/c_i$. Repeating this procedure for the other two islands leads to two more equations of type (64). Hence, we obtain a system of equations of three equations and the unknowns $c_1$, $c_2$, and $c_3$. The system of equations

$$\mathbf{\Gamma} \cdot \begin{pmatrix} c_1 \\ c_2 \\ c_3 \end{pmatrix} = \begin{pmatrix} \gamma_I^1 \\ \gamma_I^2 \\ \gamma_I^3 \end{pmatrix}, \tag{65}$$

where matrix $\mathbf{\Gamma}$ contains all $\gamma_B^{ij*}$, is solved by matrix inversion.

$\Psi_B^{i*}$ and $\bar{\mathbf{u}}_\mathbf{B}^{i*}$ are calculated in `ubarsolv.F`. The path integrals $\gamma_I^j$ and $\gamma_B^{ij*}$ are calculated in `island.F`. The inversion of $\mathbf{\Gamma}$ is calculated in `matinv.F`, and the following matrix multiplication to determine the constants is performed in subroutine `matmult` in `matinv.F`. $\Psi$ and $\bar{\mathbf{u}}$ are finally calculated in `mains.F`.

Concerning the discretization of the path integral (61), the discretization of the following components are noteworthy:

$$f\bar{v} = f\frac{\bar{v}_{i,j} + \bar{v}_{i+1,j} + \bar{v}_{i,j-1} + \bar{v}_{i+1,j-1}}{4} \tag{66}$$

and analogously

$$f\bar{u} = f\frac{\bar{u}_{i-1,j} + \bar{u}_{i,j} + \bar{u}_{i-1,j+1} + \bar{u}_{i,j+1}}{4} \tag{67}$$

(see Fig. 11). Note that this non-weighted averaging in latitudinal direction is valid because we are in $\sin\theta$ space.

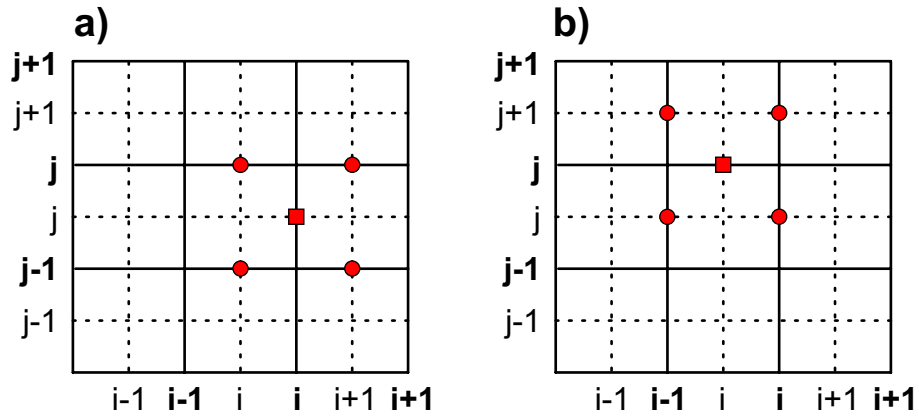


**Figure 11:** Visualization of the discretization of a) Eq. (66) where $\bar{v}$ is transformed onto the u-grid and b) Eq. (67) where $\bar{u}$ is transformed on to the v-grid.

### 2.2.8 u, v, and w

`velc.F`

The three-dimensional velocity fields $u$ and $v$, i.e. the sum of the barotropic and the baroclinic horizontal velocities, are calculated in `velc.F`. Afterwards, the velocity relaxation (Eq. 13) is calculated.

The vertical velocity component $w$ follows from the Continuity Equation (12) which can be written as:

$$\nabla \cdot \mathbf{u} = \frac{1}{r}\frac{\partial}{\partial \phi}\frac{1}{\cos\theta}u + \frac{1}{r}\frac{\partial}{\partial(\sin\theta)}\cos\theta v + \frac{\partial}{\partial z}w = 0. \tag{68}$$

The solution of the discretized version of Eq. (68) is

$$w_{i,j,k} = w_{i,j,k-1} - (\Delta z)^e_k \left( \frac{u_{i,j,k} - u_{i-1,j,k}}{r\Delta\phi\cos\theta^u_j} + \frac{\cos\theta^v_j v_{i,j,k} - \cos\theta^v_{j-1} v_{i,j-1,k}}{r(\Delta\sin\theta)} \right). \tag{69}$$

The vertical component of the velocity is zero at the sea floor: $w_{i,j,\mathrm{kmin}} = 0\ \mathrm{m\,s^{-1}}$. See also Fig. 12.

# 3 Transport equation for tracers

`tstivpo.F`

The transport equation for tracers $X$ reads

$$\frac{D}{Dt}X = \frac{\partial}{\partial t}X + \nabla\cdot(\mathbf{u}X) = \nabla(\mathbf{A}\nabla X) + \mathbf{C}X + \mathrm{SMS}, \tag{70}$$

where $\mathbf{C}$ stands for the convective adjustment operator and SMS represents source-minus-sink terms such as net air-sea fluxes or radioactive decay [Müller et al., 2006]. For the

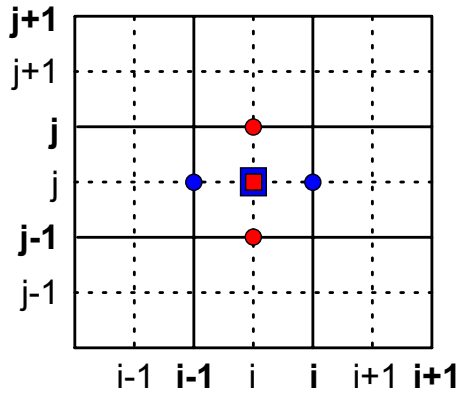


**Figure 12:** Visualization of the discretization of the derivatives of $u$ and $v$ of Eqs. (69). Blue circles denote zonal velocities $u$, the blue square the derivative of $u$, red squares the meridional velocities $v$, and the red square the derivative of $v$.

advective term the velocity $\mathbf{u}$ is used as calculated from the frictional geostrophic balance equations (9 - 11).

$$\mathbf{A} = \begin{pmatrix} K_I & 0 & (K_I - \kappa)S_\phi \\ 0 & K_I & (K_I - \kappa)S_\theta \\ (K_I + \kappa)S_\phi & (K_I + \kappa)S_\theta & K_I\mathbf{S}^2 + K_D \end{pmatrix} \tag{71}$$

is the diffusive mixing tensor with $K_I$ and $K_D$ the isopycnal and diapycnal diffusivities, respectively, $\kappa$ the Gent-McWilliams parameter which parametrizes sub-scale eddies, and

$$\mathbf{S} = (S_\phi, S_\theta, 0) = \left( -\frac{1}{r\cos\theta}\frac{\frac{\partial\rho}{\partial\phi}}{\frac{\partial\rho}{\partial z}}, -\frac{\cos\theta}{r}\frac{\frac{\partial\rho}{\partial(\sin\theta)}}{\frac{\partial\rho}{\partial z}}, \quad 0 \right) \tag{72}$$

the local slope of the isopycnals.

In the Bern3D model, the tracer equation is solved in three steps. First, advection, isopycnal diffusion and the source-minus-sink terms are calculated using explicit discretization schemes. For reasons of computational efficiency, diapycnal diffusion (element $A^{33}$ of mixing tensor $\mathbf{A}$) is solved implicitly from the resulting tracer field (see Müller [2007] for details). In the third step, convection is calculated from the resulting tracer field.

## 3.1 Discretization part 1

The transport equation (70) for advection, isopycnal diffusion and source-minus-sink terms can be written as follows:

$$\frac{\partial}{\partial t}X = -\frac{1}{r}\frac{\partial}{\partial\phi}\frac{1}{\cos\theta}F^u - \frac{1}{r}\frac{\partial}{\partial(\sin\theta)}\cos\theta F^v - \frac{\partial F^w}{\partial z} + \text{SMS}, \tag{73}$$

where $F^u$, $F^v$, and $F^w$ are advective and diffusive fluxes in zonal, meridional, and vertical direction, respectively. The discretized version of this equation is

$$\begin{aligned} X^{t+\Delta t}_{i,j,k} =& X^t_{i,j,k} - \Delta t \left[ \frac{1}{r\Delta\phi \cos\theta^u_j} (F^u_{i,j,k} - F^u_{i-1,j,k}) \right. \\ &+ \frac{1}{r\Delta(\sin\theta)} (\cos\theta^v_j F^v_{i,j,k} - \cos\theta^v_{j-1} F^v_{i,j-1,k}) \\ &\left. + \frac{1}{\Delta z^e_k} (F^w_{i,j,k} - F^w_{i,j,k-1}) - \mathrm{SMS}_{i,j,k} \right]. \end{aligned} \tag{74}$$

In the model code, the fluxes are denoted eastern, western, northern, southern boundary fluxes and fluxes above and below the cell with $F^E_{i,j,k} = \frac{1}{\cos\theta^u_j} F^u_{i,j,k}$, $F^W_{i,j,k} = \frac{1}{\cos\theta^u_j} F^u_{i-1,j,k}$, $F^N_{i,j,k} = \cos\theta^v_j F^v_{i,j,k}$, $F^S_{i,j,k} = \cos\theta^v_{j-1} F^v_{i,j-1,k}$, $F^a_{i,j,k} = F^w_{i,j,k}$, and $F^b_{i,j,k} = F^w_{i,j,k-1}$. Hence,

$$\begin{aligned} X^{t+\Delta t}_{i,j,k} =& X^t_{i,j,k} - \Delta t \left[ \frac{1}{r\Delta\phi} (F^E_{i,j,k} - F^W_{i,j,k}) \right. \\ &+ \frac{1}{r\Delta(\sin\theta)} (F^N_{i,j,k} - F^S_{i,j,k}) \\ &\left. + \frac{1}{\Delta z^e_k} (F^a_{i,j,k} - F^b_{i,j,k}) - \mathrm{SMS}_{i,j,k} \right]. \end{aligned} \tag{75}$$

### 3.1.1 Advection

The advective term of Eq. (70),

$$\nabla \cdot (\mathbf{u}X) = \frac{1}{r} \frac{\partial}{\partial\phi} \frac{1}{\cos\theta} uX + \frac{1}{r} \frac{\partial}{\partial(\sin\theta)} \cos\theta vX + \frac{\partial}{\partial z} wX \tag{76}$$

is discretized by averaging $X$ onto the velocity grid by using the variable upstream-weighting scheme described by Fiadeiro and Veronis [1977]:

$$\begin{aligned} \nabla \cdot (\mathbf{u}X) =& \frac{1}{r\Delta\phi \cos\theta^u_j} (u_{i,j,k} X^u_{i,j,k} - u_{i-1,j,k} X^u_{i-1,j,k}) \\ &+ \frac{1}{r\Delta(\sin\theta)} (\cos\theta^v_j v_{i,j,k} X^v_{i,j,k} - \cos\theta^v_{j-1} v_{i,j-1,k} X^v_{i,j-1,k}) \\ &+ \frac{1}{(\Delta z)^e_k} (w_{i,j,k} X^w_{i,j,k} - w_{i,j,k-1} X^w_{i,j,k-1}), \end{aligned} \tag{77}$$

with

$$X^u_{i,j,k} = \frac{1}{2} \left[ \left( 1 + \frac{\mathrm{Pec}^u_{i,j,k}}{|\mathrm{Pec}^u_{i,j,k}| + 2} \right) X_{i,j,k} + \left( 1 - \frac{\mathrm{Pec}^u_{i,j,k}}{|\mathrm{Pec}^u_{i,j,k}| + 2} \right) X_{i+1,j,k} \right] \tag{78}$$

and

$$\mathrm{Pec}^u_{i,j,k} = \frac{u_{i,j,k} (\Delta x)^c_j}{K_I} \tag{79}$$

the Peclet number, and analogously in $v$- and $w$-direction using

$$\mathrm{Pec}^v_{i,j,k} = \frac{v_{i,j,k}(\Delta y)^c_j}{K_I}, \tag{80}$$

and

$$\mathrm{Pec}^w_{i,j,k} = \frac{w_{i,j,k}(\Delta z)^c_k}{K_D}. \tag{81}$$

$(\Delta x)^c_j$, $(\Delta y)^c_j$, and $(\Delta z)^c_k$ denote the distance between the centers of the grid cells in $x$, $y$, and $z$ direction, respectively.

The advective boundary fluxes of cell $(i, j, k)$ are hence

$$\begin{aligned}
F^{E,\mathrm{adv}}_{i,j,k} =& \frac{1}{\cos\theta^u_j} u_{i,j,k} X^u_{i,j,k} \\
F^{W,\mathrm{adv}}_{i,j,k} =& \frac{1}{\cos\theta^u_j} u_{i-1,j,k} X^u_{i-1,j,k} \\
F^{N,\mathrm{adv}}_{i,j,k} =& \cos\theta^v_j v_{i,j,k} X^v_{i,j,k} \\
F^{S,\mathrm{adv}}_{i,j,k} =& \cos\theta^v_{j-1} v_{i,j-1,k} X^v_{i,j-1,k} \\
F^{a,\mathrm{adv}}_{i,j,k} =& w_{i,j,k} X^w_{i,j,k} \\
F^{b,\mathrm{adv}}_{i,j,k} =& w_{i,j,k-1} X^w_{i,j,k-1}.
\end{aligned} \tag{82}$$

### 3.1.2 Isopycnal diffusion

In the explicit diffusion term, $\nabla \cdot (\hat{\mathbf{A}} \nabla X)$ with $\hat{A}^{33} = 0$ and $\hat{A}^{nm} = A^{nm}$ otherwise, is discretized. The term is written out as

$$\begin{aligned}
-\nabla \cdot (\hat{\mathbf{A}} \nabla X) =& \nabla \cdot \mathbf{F}^{\mathrm{diff}} \\
=& -\frac{1}{r}\frac{\partial}{\partial\phi}\frac{1}{\cos\theta}\left(K_I \frac{1}{r\cos\theta}\frac{\partial}{\partial\phi}X + (K_I - \kappa) S_\phi \frac{\partial}{\partial z}X\right) \\
& -\frac{1}{r}\frac{\partial}{\partial(\sin\theta)}\cos\theta\left(K_I \frac{\cos\theta}{r}\frac{\partial}{\partial(\sin\theta)}X + (K_I - \kappa) S_\theta \frac{\partial}{\partial z}X\right) \\
& -\frac{\partial}{\partial z}\left((K_I + \kappa) S_\phi \frac{1}{r\cos\theta}\frac{\partial}{\partial\phi}X + (K_I + \kappa) S_\theta \frac{\cos\theta}{r}\frac{\partial}{\partial(\sin\theta)}X\right).
\end{aligned} \tag{83}$$

The first zonal diffusivity term of Eq. (83) is discretized using the centered-in-space scheme. The second term is more complicated, because the zonal flux is located on the u-grid, whereas the discretizations of $\partial X/\partial z$ and the isopycnal slope $S_\phi$ (Eq. 72) are located on the w-grid:

The derivatives of $\rho = e_1 T + e_2 S + e_3 T^2 + e_4 T^3$ [Winton and Sarachik, 1993] can be written as

$$\frac{\partial\rho}{\partial a} = \frac{\partial\rho}{\partial T}\frac{\partial T}{\partial a} + \frac{\partial\rho}{\partial S}\frac{\partial S}{\partial a} \tag{84}$$

with $a \in \{\phi, \sin\theta, z\}$,

$$\frac{\partial \rho}{\partial T} = e_1 + 2e_3 T + 3e_4 T^2, \tag{85}$$

and

$$\frac{\partial \rho}{\partial S} = e_2. \tag{86}$$

In order to convert Eq. (85) from the c-grid on to the u-grid, the adjacent temperatures are averaged: $T^u_{i,j,k} = 1/2 \cdot (T^c_{i+1,j,k} + T^c_{i,j,k})$. Thus, the discretization of $\partial\rho/\partial\phi$ is located on the u-grid. In the case of $\partial\rho/\partial z$, however, $\partial\rho/\partial T$ is located on the u-grid, but $\partial T/\partial z$ (and $\partial S/\partial z$) are located on the w-grid. The problem is solved by calculating $S_\phi \cdot (\partial X/\partial z)$ at the four grid points on the w-grid surrounding the particular u-grid point and averaging the four (see Fig. 13). If a w-grid point is located at an ocean margin, $S_\phi$ at this grid point is set to 0. Note that the slope $S_\phi$ is damped by a factor $S_{\text{lim}} = \zeta$ if it exceeds a maximum slope $S_{\max}$. Otherwise, $S_{\text{lim}} = 1$ (see Müller [2007] for more info). Hence, together with the first zonal diffusivity term,

$$F^{E,\text{diff}}_{i,j,k} = -\frac{K_I^{i,j,k}}{r\cos^2\theta^u_j \Delta\phi}(X_{i+1,j,k} - X_{i,j,k}) - (K_I^{i,j,k} - \kappa^{i,j,k})\frac{1}{4} S_{\text{lim}} \sum_{n=1}^{4} \underbrace{-\frac{1}{r\cos\theta^u_j} \frac{\frac{\partial\rho}{\partial\phi}\Big|^u_{i,j,k}}{\frac{\partial\rho}{\partial z}\Big|^w_n}}_{S^w_{\phi,n}} \frac{\partial X}{\partial z}\Big|^w_n, \tag{87}$$

where the index $n$ represents the combination of indices $(i, j, k)$ on the w-grid that surround a particular point on the u-grid. The indices $u$ and $w$ indicate on which grid the particular element is discretized (either u- or w-grid). Note that the second term of Eq. (87) can be simplified by factoring out $\frac{\partial\rho}{\partial\phi}|^u_{i,j,k}/(r\cos\theta^u_j)$ and by canceling the two minus signs. The derivative of $X$ with respect to $z$ is discretized as

$$\frac{\partial X}{\partial z}\Big|_{i,j,k} = \frac{1}{\Delta z^c_k}(X_{i,j,k+1} - X_{i,j,k}). \tag{88}$$

The western boundary flux is equal to the eastern boundary flux of the cell to the west:

$$F^{W,\text{diff}}_{i,j,k} = F^{E,\text{diff}}_{i-1,j,k}. \tag{89}$$

The discretization of the meridional diffusive flux of Eq. (83) is done analogously to the zonal diffusive flux:

$$F^{N,\text{diff}}_{i,j,k} = -\frac{K_I^{i,j,k}\cos^2\theta^v_j}{r\Delta(\sin\theta)}(X_{i,j+1,k} - X_{i,j,k}) - (K_I^{i,j,k} - \kappa^{i,j,k})\frac{1}{4} S_{\text{lim}} \sum_{n=1}^{4} S^w_{\theta,n} \frac{\partial X}{\partial z}\Big|_n. \tag{90}$$

Again, the index $n$ represents the combination of indices $(i, j, k)$ on the w-grid that surround a particular point on the v-grid.

The southern boundary flux is equal to the northern boundary flux of the cell to the south:

$$F^{S,\text{diff}}_{i,j,k} = F^{N,\text{diff}}_{i,j-1,k}. \tag{91}$$

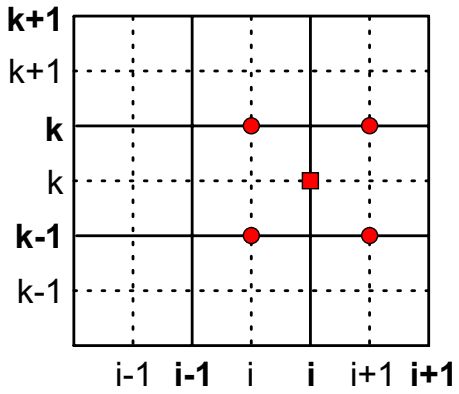


**Figure 13:** Visualization of the averaging done to transform the discretizations of $S_\phi(\partial X/\partial z)$ (circles; Eq. 83) from the w-grid onto the u-grid (square).

The vertical diffusive boundary fluxes of Eq. (83) are discretized similarly to the zonal and meridional boundary fluxes:

$$F^{a,\mathrm{diff}}_{i,j,k} = (K_I^{i,j,k} + \kappa^{i,j,k})\frac{1}{4}S_{\lim} \cdot \frac{\sum_{n=1}^{4} \frac{1}{r\cos\theta^u_j}\left.\frac{\partial\rho}{\partial\phi}\right|^u_n \frac{1}{r\cos\theta^u_j}\left.\frac{\partial X}{\partial\phi}\right|^u_n + \sum_{m=1}^{4} \frac{\cos\theta^v_m}{r}\left.\frac{\partial\rho}{\partial(\sin\theta)}\right|^v_m \frac{\cos\theta^v_m}{r}\left.\frac{\partial X}{\partial(\sin\theta)}\right|^v_m}{\left.\frac{\partial\rho}{\partial z}\right|^w_{i,j,k}} \cdot \left.\frac{\partial X}{\partial z}\right|^w_{i,j,k}. \tag{92}$$

Note that in this equation the slopes $S_\phi$ and $S_\theta$ are replaced by their elements (Eq. 72). Again, the indices $n$ and $m$ represent the combination of indices $(i, j, k)$ on the u- and v-grid that surround a particular point on the w-grid.

The boundary flux below the cell is equal to the boundary flux above the cell of the cell below:

$$F^{b,\mathrm{diff}}_{i,j,k} = F^{a,\mathrm{diff}}_{i,j,k-1}. \tag{93}$$

## 3.2 Discretization part 2 – diapycnal diffusion

The diffusive transport that arises from element $A_{33}$ of the mixing tensor (71) is accounted for after the mixing that arises from the other elements is calculated. Because this element would require a substantially smaller time step than the other elements in an explicit discretization scheme, it is solved implicitly (see Müller [2007] for details). The equation to be solved is

$$\frac{\partial}{\partial t}X = \frac{\partial}{\partial z}(K_D + K_I\mathbf{S}^2)\frac{\partial}{\partial z}X. \tag{94}$$

Using $\xi = K_D + K_I\mathbf{S}^2$, the implicit discretized form of this equation is

$$X^{t+\Delta t}_{i,j,k} = \frac{\Delta t}{(\Delta z)^e_k}\left[\frac{\xi_{i,j,k}}{(\Delta z)^c_k}(X^{t+\Delta t}_{i,j,k+1} - X^{t+\Delta t}_{i,j,k}) - \frac{\xi_{i,j,k-1}}{(\Delta z)^c_{k-1}}(X^{t+\Delta t}_{i,j,k} - X^{t+\Delta t}_{i,j,k-1})\right] + X^t_{i,j,k} \tag{95}$$

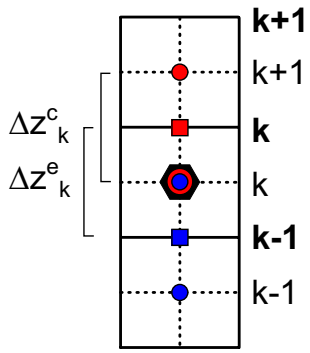


**Figure 14:** Visualization of the discretization of Eq. (95). The circles denote the tracer concentrations $X$, the squares denote the first derivatives that are calculated from the tracer concentrations (circles) of the same color. The polygon denotes the second derivative that is calculated from the first order derivatives (squares).

(see also Fig. 14). In matrix form Eq. (95) reads

$$\mathbf{M_{i,j}} \cdot \begin{pmatrix} X^{t+\Delta t}_{i,j,\mathrm{kmin}(i,j)} \\ X^{t+\Delta t}_{i,j,\mathrm{kmin}(i,j)+1} \\ \vdots \\ X^{t+\Delta t}_{i,j,\mathrm{kmax}} \end{pmatrix} = \begin{pmatrix} X^{t}_{i,j,\mathrm{kmin}(i,j)} \\ X^{t}_{i,j,\mathrm{kmin}(i,j)+1} \\ \vdots \\ X^{t}_{i,j,\mathrm{kmax}} \end{pmatrix} \tag{96}$$

with

$$\mathbf{M_{i,j}} = \begin{bmatrix} 1+\frac{\Delta t}{(\Delta z)^e_{\mathrm{kmin}}}\frac{\xi_{\mathrm{kmin}}}{(\Delta z)^c_{\mathrm{kmin}}} & -\frac{\Delta t}{(\Delta z)^e_{\mathrm{kmin}}}\frac{\xi_{\mathrm{kmin}}}{(\Delta z)^c_{\mathrm{kmin}}} & 0 & \cdots & 0 \\ -\frac{\Delta t}{(\Delta z)^e_{\mathrm{kmin}+1}}\frac{\xi_{\mathrm{kmin}}}{(\Delta z)^c_{\mathrm{kmin}}} & 1+\frac{\Delta t}{(\Delta z)^e_{\mathrm{kmin}+1}}\left(\frac{\xi_{\mathrm{kmin}+1}}{(\Delta z)^c_{\mathrm{kmin}+1}}+\frac{\xi_{\mathrm{kmin}}}{(\Delta z)^c_{\mathrm{kmin}}}\right) & -\frac{\Delta t}{(\Delta z)^e_{\mathrm{kmin}+1}}\frac{\xi_{\mathrm{kmin}+1}}{(\Delta z)^c_{\mathrm{kmin}+1}} & 0 & \\ 0 & \ddots & \ddots & \ddots & \ddots \\ \vdots & \ddots & \ddots & \ddots & \end{bmatrix}. \tag{97}$$

Note that the diffusivities $K_I$ and $K_D$ are zero at the sea surface and at the sea floor. Matrix $\mathbf{M_{i,j}}$ must be solved for every water column $(i, j)$. $\mathrm{kmin}(i, j)$ is the k-index of the bottom-most wet cell of column $(i, j)$ (the sea floor), and kmax is the k-index at the sea surface. $\mathbf{M_{i,j}}$ is a tridiagonal matrix of the form

$$\mathbf{M} = \begin{bmatrix} b_1 & c_1 & 0 & \cdots & & & \\ a_2 & b_2 & c_2 & \cdots & & & \\ & & & \cdots & a_{N-1} & b_{N-1} & c_{N-1} \\ & & & \cdots & 0 & a_N & b_N \end{bmatrix} \tag{98}$$

that can be inverted efficiently using a special algorithm for the LU-decomposition of tridiagonal matrices. The algorithm is given in Press et al. [1986]. In this algorithm, the

diagonal elements are stored in vectors **a**, **b**, and **c** (with $a_{\mathrm{kmin}(i,j)} = 0$ and $c_{\mathrm{kmax}} = 0$). Thus, the many zeros of matrix $\mathbf{M_{i,j}}$ need not be stored.

## 3.3 Discretization part 3 – convection

Convection is calculated from the resulting tracer field after advection and diffusion is calculated. It occurs when dense water overlies water with a lower density. Convection mixes the water column until the density increases monotonically over depth. In the Bern3D model, two types of convection are calculated. The first type is referred to as shuffling convection, the second type that follows the shuffling convection is referred to as mixing convection. In the transport equation (70) they are summed up in operator **C**. Both convection algorithms cannot be described analytically. They are characterized in the following.

### 3.3.1 Shuffling convection

`coshuffle.F`

In the shuffling convection scheme, dense surface waters sink down to depth until the surrounding waters are of equal density. The water parcel is not mixed on its way down (Fig. 15). The shuffling is repeated until the surface cell is no longer denser than the underlying cell. This scheme has been introduced because mixing convection alone leads to a too large uptake of tracers, especially due to water column instabilities caused by the seasonal cycle [Müller, 2007]. Note that in the current standard version of the model, shuffling convection is only applied to temperature and salinity, but not to other tracers.

### 3.3.2 Mixing convection

`co.F`

Mixing convection mixes superposed cells if the overlying cell is of greater density than the cells below (see Fig. 16). After the mixing, the density in the water column increases monotonically with depth.

# A Averaging in z-direction

Quantities on the c-grid are averaged on to the w-grid in Eqs. (31) and (42). Because the grid-cell height increases with depth, a weighted-averaging must be performed to average values from the c-grid on to the w-grid:

$$X_k^w = \frac{X_{k+1}(z_k^c - z_k^w) + X_k(z_k^w - z_{k+1}^c)}{z_k^c - z_{k+1}^c} \tag{99}$$

(Fig. 17). However, in the case of the exponential distribution of the cell-heights in the Bern3D model (Eqs. 1 and 2), the weighted-averaging can be simplified to a non-weighted averaging in second-order approximation. This is shown in the following.

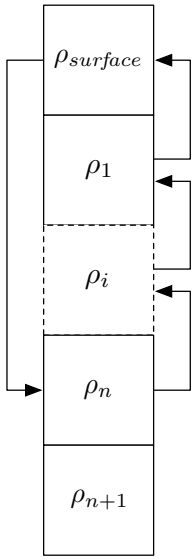


**Figure 15:** Shuffling convection scheme. If the density of the surface cell ($\rho_{\text{surface}}$) is higher than the density of the cells below, then the contents of the surface cell are moved to cell $n$, where $\rho_n < \rho_{\text{surface}}$ and $\rho_{n+1} \geq \rho_{\text{surface}}$. The contents of the cells 1 to $n$ are shifted upwards. These steps are repeated as long as $\rho_{\text{surface}} > \rho_1$. Mass is preserved during the movement process. Figure from Ritz [2007].

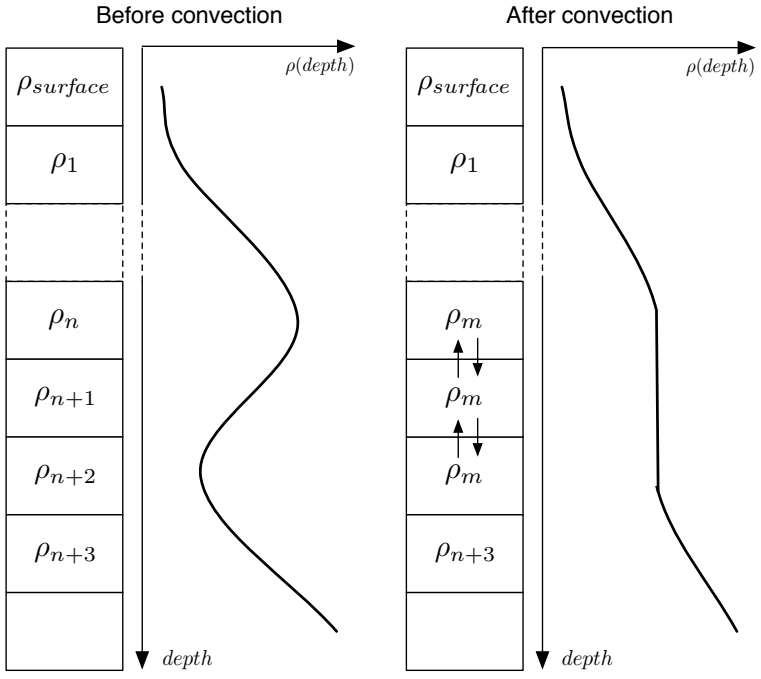


**Figure 16:** Mixing convection scheme. This convection scheme is calculated after the shuffling convection. Superposed cells $n$, $n+1$, ... with $\rho_n > \rho_{n+1} > \ldots$ are mixed such that in the end these cells are all of equal density while preserving mass. This step is repeated until $\rho_{\text{surface}} > \rho_1 > \ldots > \rho_i \forall i$. Figure from Ritz [2007].

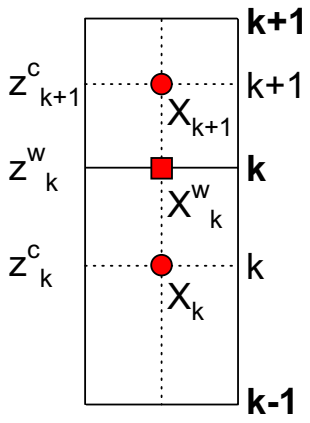


**Figure 17:** Visualization of the averaging done in z-direction (Eq. 99). The red circles denote values on the c-grid, the red square is the averaged value on the w-grid. Note that the cells are not of equal height. Also, the c-gridpoints are not located in the center of the cells.

$z_k^w$ is of the form

$$z_k^w = \eta(a^x - 1) \tag{100}$$

with $a = 1 + 1/\eta$ and $x = (\text{kmax} - k)/\text{kmax}$. The same is true for $z_k^c$ with $x = (\text{kmax} - k + 0.5)/\text{kmax}$. The Taylor expansion of $a^x$ is

$$a^x = 1 + (\log a)x + O(x^2). \tag{101}$$

When Eqs. (100) and (101) are substituted into Eq. (99), the equation reads

$$X_k^w \approx \frac{X_{k+1} + X_k}{2} \tag{102}$$

which is a non-weighted average. Note that in the third-order approximation, Eq. (99) becomes a weighted average. In this case an additional term is added to the Taylor expansion:

$$a^x = 1 + (\log a)x + \frac{(\log a)^2}{2}x^2 + O(x^3). \tag{103}$$

Eq. (99) then reads:

$$X_k^w \approx \frac{X_{k+1}\left(\frac{1}{2} + \frac{\log a(0.25+\text{kmax}-k)}{2\text{kmax}}\right) + X_k\left(\frac{1}{2} + \frac{\log a(-0.25+\text{kmax}-k)}{2\text{kmax}}\right)}{1 + \frac{\log a(\text{kmax}-k)}{\text{kmax}}}. \tag{104}$$

# References

N. R. Edwards and R. Marsh. Uncertainties due to transport-parameter sensitivity in an efficient 3-D ocean-climate model. *Climate Dynamics*, 24:415–433, 2005.

N. R. Edwards and J. G. Shepherd. Bifurcations of the thermohaline circulation in a simplified three-dimensional model of the world ocean and the effects of inter-basin connectivity. *Climate Dynamics*, 19:31–42, 2002.

N. R. Edwards, A. J. Willmott, and P. D. Killworth. On the role of topography and wind stress on the stability of the thermohaline circulation. *Journal of Physical Oceanography*, 28:756–778, 1998.

M. E. Fiadeiro and G. Veronis. On weighted-mean schemes for the finite-difference approximation to the advection-diffusion equation. *Tellus*, 29:512–522, 1977.

S. A. Müller. *Large-scale ocean circulation, air-sea gas exchange, and carbon isotopes in a three-dimensional, computationally efficient ocean model*. PhD thesis, University of Bern, Bern, Switzerland, 2007.

S. A. Müller, F. Joos, N. R. Edwards, and T. F. Stocker. Water mass distribution and ventilation time scales in a cost-efficient, three-dimensional ocean model. *Journal of Climate*, 19:5479–5499, 2006.

W. H. Press, B. P. Flannery, S. A. Teukolsky, and W. T. Vetterling. *Numerical Recipes - The art of scientific computing*. Cambridge University Press, New York, USA, 1986.

S. P. Ritz. Global distribution of radiocarbon during changes of the Atlantic meridional overturning circulation. Master's thesis, University of Bern, Bern, Switzerland, 2007.

S. P. Ritz. *Development of a reduced-complexity climate model and applications on glacial-interglacial timescales*. PhD thesis, University of Bern, Bern, Switzerland, 2011.

S. P. Ritz, T. F. Stocker, and F. Joos. A coupled dynamical ocean - energy balance atmosphere model for paleoclimate studies. *Journal of Climate*, 24:349–375, 2011a.

S. P. Ritz, T. F. Stocker, and J. P. Severinghaus. Noble gases as proxies of mean ocean temperature: sensitivity studies using a climate model of reduced complexity. *Quaternary Science Reviews*, 30:3728–3741, 2011b.

T. F. Stocker. *Introduction to Climate Modelling*. Advances in Geophysical and Environmental Mechanics and Mathematics. Springer-Verlag Berlin Heidelberg, first edition, 2011.

L. D. Talley, G. L. Pickard, W. J. Emery, and J. H. Swift. *Descriptive Physical Oceanography: An Introduction*. Academic Press, London, sixth edition, 2011.

M. Winton and E. S. Sarachik. Thermohaline oscillations induced by strong steady salinity forcing of ocean general-circulation models. *Journal of Physical Oceanography*, 23(7): 1389–1410, 1993.